Available online at www.sciencedirect.com
ScienceDirect
Journal of Sound and Vibration 318 (2008) 725–736
JOURNAL OF SOUND AND VIBRATION
www.elsevier.com/locate/jsvi

Active vibration isolation and underwater sound radiation control

Zhiyi Zhang*, Yong Chen, Xuewen Yin, Hongxing Hua

Institute of Vibration, Shock and Noise, Shanghai Jiaotong University, Shanghai 200240, PR China

Received 2 November 2007; received in revised form 12 April 2008; accepted 16 April 2008
Handling Editor: J. Lam
Available online 3 June 2008

Abstract

Active vibration isolation and underwater sound radiation of structures are presented to investigate issues relevant to vibration control and far-field sound radiation of underwater structures. Finite element method (FEM) and boundary element method (BEM) are combined to model fluid–structure coupled systems. In the modeling of fluid–structure interaction, mode truncation and inertial coupling between fluid and structures are applied to sufficiently reduce model order. Moreover, the added mass matrix of fluid is modified to increase the accuracy of computation of natural frequencies of the coupled system. The modeling approach is presented especially for constructing time-domain models, which are inherently more suitable for exploring active control strategies than frequency-domain models for complicated and especially nonlinear systems. Adaptive control with two different weight updating algorithms is discussed. One is based on the local vibration and the other on the summed vibration. In the simulation example, a model of two degrees of freedom connected to a rigidly baffled plate with stiffeners is used to demonstrate the difference between active isolation of vibration and the suppression of far-field sound radiation, and it is demonstrated that suppression of summed vibration can result in smaller sound radiation than the suppression of local vibration only.

1. Introduction

Structure-borne sound has been deeply investigated. Analyses on structural vibration and the relevant sound radiation in light or heavy fluid medium occurred as early as in the 1950s [1–4], but the research about active control of structural sound radiation started in the late 1980s [5–8], which is mainly attributed to the development of high-speed computation technologies and the impetus of industrial applications. Compared with the research of sound radiation in air, there is little work about underwater sound radiation control [9]. In the analysis of structural sound radiation, finite element method (FEM) and FEM/boundary element method (BEM) are widely used to deal with fluid–structure interaction, and especially FEM/BEM is the preferable method due to its advantage in reducing the degrees of freedom (DOFs) of coupled systems [10–13]. For steady-state sound radiation problems, fluid–structure interaction is usually treated in the frequency domain

*Corresponding author.
E-mail address: chychang@sjtu.edu.cn (Z. Zhang).

0022-460X/$ - see front matter © 2008 Elsevier Ltd. All rights reserved.
doi:10.1016/j.jsv.2008.04.027

with consideration of fluid compressibility and accordingly the wave equation is replaced by the Helmholtz differential equation. However, the transient fluid–structure interaction such as structural responses to underwater explosion should be described with time-domain methods, in which doubly asymptotic approximations are the well-known techniques and used as well in the prediction of structural sound radiation [14,15]. So far, all the work about active vibration isolation has only considered how to effectively control structural vibration whereas fluid–structure interaction as well as the resulting sound radiation has not yet been involved. In order to investigate active vibration isolation and the related underwater structural sound radiation in the time domain, a lower order model with accurate description of dynamics at the low–medium frequencies is then necessary to numerical simulation. In this paper, an approximate description of fluid–structure interaction is given by neglecting the compressibility of fluid. As a result, the wave equation is degraded to the Laplace equation. In the modeling, lumped parameter method and the FEM are combined to derive structural vibration models, and the BEM is used to describe wave motion in the fluid. Normal accelerations at the interfaces of fluid and structures are regarded as known variables. Hence, only inertial coupling between fluid and structures is considered, which reduces the DOFs of the coupled system. Moreover, the added mass matrix of the fluid is modified in order to guarantee the accuracy of computed natural frequencies as well as the low-frequency characteristics of the coupled system.

In Section 2, motion equation of the fluid–structure coupled system is established. A reduced modal model of the flexible structure is obtained by FEM and synthesized with the boundary element model of the fluid to derive the coupled system model. In Section 3, active control strategies are discussed, and especially, two different adaptive algorithms are given for the adaptive control of the far-field sound radiation. Section 4 gives an example to demonstrate the validity of the modeling approach. Based on this model, active vibration isolation and the relevant far-field sound radiation are simulated in Section 5 with 2-DOF vibration model mounted on a rigidly baffled plate with stiffeners and relations between active vibration isolation and the sound radiation are illustrated. Finally, in Section 6, concluding remarks are given.

2. Mathematical description

Consider the fluid–structure coupled system shown in Fig. 1. As illustrated, S_1 is the vibration source, S_2 is the flexible structure that radiates sound into the surrounding fluid and coupled with the fluid on its outer surface. S_1 and S_2 are coupled through springs, dampers and actuators.

Suppose S_1 is described with a lumped parameter model, S_2 with a finite element model and the fluid with a boundary element model. The vibration equations of S_1 and S_2 are given as follows:

$$\begin{bmatrix} M_{1i} & M_{1c} \\ M_{1c}^{\mathrm{T}} & M_{1f} \end{bmatrix} \begin{Bmatrix} \ddot{x}_{1i} \\ \ddot{x}_{1f} \end{Bmatrix} + \begin{bmatrix} D_{1i} & D_{1c} \\ D_{1c}^{\mathrm{T}} & D_{1f} \end{bmatrix} \begin{Bmatrix} \dot{x}_{1i} \\ \dot{x}_{1f} \end{Bmatrix} + \begin{bmatrix} K_{1i} & K_{1c} \\ K_{1c}^{\mathrm{T}} & K_{1f} \end{bmatrix} \begin{Bmatrix} x_{1i} \\ x_{1f} \end{Bmatrix} = \begin{Bmatrix} F_{1i} \\ F_{1f} \end{Bmatrix}, \tag{1}$$

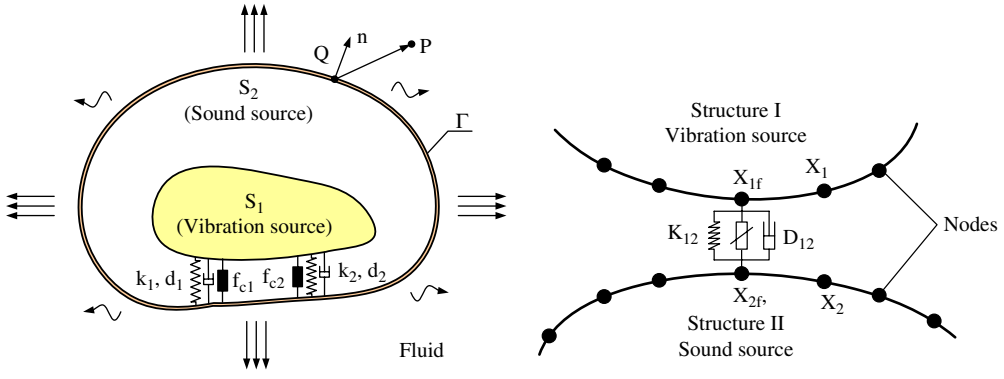

Fig. 1. Active vibration isolation and sound radiation of underwater structures.

$$\begin{bmatrix} M_{2f} & M_{2c} \\ M_{2c}^{\mathrm{T}} & M_{2i} \end{bmatrix} \begin{Bmatrix} \ddot{x}_{2f} \\ \ddot{x}_{2i} \end{Bmatrix} + \begin{bmatrix} D_{2f} & D_{2c} \\ D_{2c}^{\mathrm{T}} & D_{2i} \end{bmatrix} \begin{Bmatrix} \dot{x}_{2f} \\ \dot{x}_{2i} \end{Bmatrix} + \begin{bmatrix} K_{2f} & K_{2c} \\ K_{2c}^{\mathrm{T}} & K_{2i} \end{bmatrix} \begin{Bmatrix} x_{2f} \\ x_{2i} \end{Bmatrix} = \begin{Bmatrix} F_{2f} \\ F_{2i} \end{Bmatrix} - T\{p\}, \tag{2}$$

where $(x_{1i}^{\mathrm{T}}, x_{1f}^{\mathrm{T}})^{\mathrm{T}}$ is the displacement vector of S_1, $(x_{2i}^{\mathrm{T}}, x_{2f}^{\mathrm{T}})^{\mathrm{T}}$ the displacement vector of S_2, x_{1i} and x_{2i} the displacements of uncoupled nodes of S_1 and S_2, respectively, while x_{1f} and x_{2f} are the displacements of coupled nodes of S_1 and S_2 at those positions where springs, dampers and actuators are mounted, F_{1i} and F_{2i} are excitation forces acting on the uncoupled nodes of S_1 and S_2, respectively, F_{1f} and F_{2f} are forces acting on the coupled nodes of S_1 and S_2, respectively, $\{p\}$ is the pressure acting on the outer surface of S_2, T is the matrix converting fluid pressure to the nodal loads on S_2, the matrices on the left-hand sides of Eqs. (1) and (2) are the mass matrices, the damping matrices and the stiffness matrices, respectively, and assumed to be independent of frequency. The relation between F_{1f} and F_{2f} is given by

$$F_{2f} = -F_{1f} = K_{12}(x_{1f} - x_{2f}) + D_{12}(\dot{x}_{1f} - \dot{x}_{2f}) + F_c, \tag{3}$$

where K_{12} and D_{12} are the coupling matrices that relates displacements and velocities of S_1 and S_2, respectively, F_c is the control force vector. In order to reduce the order of the coupled system, we can express the displacement of S_2 by the responses of low-order vibration modes (in vacuo), therefore,

$$\begin{Bmatrix} x_{2f} \\ x_{2i} \end{Bmatrix} \approx \sum_{k=1}^{N} \zeta_k \phi_k = \sum_{k=1}^{N} \zeta_k \begin{Bmatrix} \phi_{fk} \\ \phi_{ik} \end{Bmatrix}, \quad \Phi = \begin{Bmatrix} \Phi_f \\ \Phi_i \end{Bmatrix} = [\,\phi_1 \quad \phi_2 \quad \cdots \quad \phi_N\,], \tag{4}$$

where N is the number of retained modes, which is far less than the dof of S_2, ζ_k the kth modal coordinate, ϕ_k the kth mode shape, Φ the matrix formed by the N mode shapes. Assume $F_{2i} = O$, in light of Eqs. (1)–(4), one can have

$$\begin{bmatrix} M_{1i} & M_{1c} & O \\ M_{1c}^{\mathrm{T}} & M_{1f} & O \\ O & O & M_z \end{bmatrix} \begin{Bmatrix} \ddot{x}_{1i} \\ \ddot{x}_{1f} \\ \ddot{Z} \end{Bmatrix} + \begin{bmatrix} D_{1i} & D_{1c} & O \\ D_{1c}^{\mathrm{T}} & D_{1f} + D_{12} & -D_{12}\Phi_f \\ O & -\Phi_f^{\mathrm{T}} D_{12} & D_z \end{bmatrix} \begin{Bmatrix} \dot{x}_{1i} \\ \dot{x}_{1f} \\ \dot{Z} \end{Bmatrix}$$
$$+ \begin{bmatrix} K_{1i} & K_{1c} & O \\ K_{1c}^{\mathrm{T}} & K_{1f} + K_{12} & -K_{12}\Phi_f \\ O & -\Phi_f^{\mathrm{T}} K_{12} & K_z \end{bmatrix} \begin{Bmatrix} x_{1i} \\ x_{1f} \\ Z \end{Bmatrix} = \begin{Bmatrix} F_{1i} \\ -F_c \\ \Phi_f^{\mathrm{T}} F_c \end{Bmatrix} - \begin{Bmatrix} O \\ O \\ \Phi^{\mathrm{T}} T p \end{Bmatrix}, \tag{5}$$

where

$$M_z = \Phi^{\mathrm{T}} \begin{bmatrix} M_{2f} & M_{2c} \\ M_{2c}^{\mathrm{T}} & M_{2i} \end{bmatrix} \Phi, \quad D_z = \Phi^{\mathrm{T}} \begin{bmatrix} D_{2f} + D_{12} & D_{2c} \\ D_{2c}^{\mathrm{T}} & D_{2i} \end{bmatrix} \Phi,$$
$$K_z = \Phi^{\mathrm{T}} \begin{bmatrix} K_{2f} + K_{12} & K_{2c} \\ K_{2c}^{\mathrm{T}} & K_{2i} \end{bmatrix} \Phi, \quad Z = \{\zeta_1, \zeta_2, \ldots, \zeta_N\}^{\mathrm{T}}.$$

Eq. (5) gives the coupled vibration of structures and fluid, in which the pressure p of the fluid should be described by the wave equation.

Suppose S_2 is submerged in an infinite body of fluid, then the sound pressure p induced by the vibration of S_2 is described by the following wave equation:

$$\nabla^2 p = \frac{1}{c^2} \frac{\partial^2 p}{\partial t^2}, \tag{6.1}$$

$$\partial p / \partial n = -\rho a(t) \quad \text{on the boundary}, \tag{6.2}$$

where ∇^2 is the Laplacian operator, c the sound speed in the fluid, ρ the fluid density, n the normal to the surface of S_2, and $a(t)$ the acceleration projected to the normal. The counterpart of Eq. (6) in the frequency

domain is the Helmholtz differential equation, which is not considered here in order to discuss the problem with time-domain methods.

To investigate active vibration isolation involving fluid–structure interaction in the time domain, Eq. (6) should be simplified so that a reduced discrete model can be derived. As usually conducted, Eq. (6) is degraded to the Laplace equation by neglecting the compressibility of fluid, i.e. the sound speed c in Eq. (6) is taken as infinity. In this circumstance, the influence of fluid on the dynamic behavior of structures is equal to adding inertial mass to the surface of S_2, which will be seen in Eq. (9). This way of simplification can substantially reduce the DOFs while the accuracy of the coupled model is retained at low frequencies. In fact, the BEM can be used to solve the Laplace equation, and the resulting fluid elements are only those on the surface of S_2. According to the Helmholtz integral equation and the supposition that the sound speed is infinite, the pressure at an arbitrary point within the fluid domain can be given by the integration on the boundary Γ (Fig. 1), i.e.

$$C(P)p(P) = \int_{\Gamma} \left(\frac{\partial g(Q,P)}{\partial n} p(Q) - g(Q,P) \frac{\partial p(Q)}{\partial n} \right) \mathrm{d}\Gamma, \tag{7.1}$$

$$C(P) = \begin{cases} 1 & P \text{ in fluid}, \\ 1/2 & P \text{ on } \Gamma, \\ 0 & \text{otherwise}, \end{cases} \qquad g(Q,P) = \frac{1}{4\pi r(Q,P)}, \tag{7.2}$$

where $p(P)$ is the pressure at P, n the normal to Γ, $g(Q, P)$ the Green's function, $r(Q, P)$ the distance from Q to P, as shown in Fig. 1. If P is also located on Γ, one can obtain from Eq. (7) the matrix relation between the pressure $\{p\}$ and the acceleration $\{\ddot{x}_2\}$ at all nodes on the boundary Γ:

$$H\{p\} = G \begin{Bmatrix} \ddot{x}_{2f} \\ \ddot{x}_{2i} \end{Bmatrix} = G\Phi\{\ddot{Z}\}. \tag{8}$$

In light of Eq. (8), Eq. (5) can be rewritten as

$$\begin{bmatrix} M_{1i} & M_{1c} & O \\ M_{1c}^{\mathrm{T}} & M_{1f} & O \\ O & O & M_z + \Phi^{\mathrm{T}} T H^{-1} G \Phi \end{bmatrix} \begin{Bmatrix} \ddot{x}_{1i} \\ \ddot{x}_{1f} \\ \ddot{Z} \end{Bmatrix} + \begin{bmatrix} D_{1i} & D_{1c} & O \\ D_{1c}^{\mathrm{T}} & D_{1f} + D_{12} & -D_{12}\Phi_f \\ O & -\Phi_f^{\mathrm{T}} D_{12} & D_z \end{bmatrix} \begin{Bmatrix} \dot{x}_{1i} \\ \dot{x}_{1f} \\ \dot{Z} \end{Bmatrix}$$
$$+ \begin{bmatrix} K_{1i} & K_{1c} & O \\ K_{1c}^{\mathrm{T}} & K_{1f} + K_{12} & -K_{12}\Phi_f \\ O & -\Phi_f^{\mathrm{T}} K_{12} & K_z \end{bmatrix} \begin{Bmatrix} x_{1i} \\ x_{1f} \\ Z \end{Bmatrix} = \begin{Bmatrix} F_{1i} \\ -F_c \\ \Phi_f^{\mathrm{T}} F_c \end{Bmatrix}, \tag{9}$$

where the mass matrix has been changed and no pressure load appears on the right-hand side.

In Eq. (9), all matrices are independent of frequency, which implies Eq. (9) is suitable for analyzing fluid–structure interaction in the time domain. The right-hand side of Eq. (9) represents the load vector acting on the coupled system, of which the disturbance force F_{1i} excites S_2 and thus generates sound in the far field while the control force F_c suppresses vibration of S_2 and thus reduces the radiated sound in the far field. From Eqs. (8) and (9), we can discuss different control strategies and obtain the variation of sound pressure in the far field before and after active vibration isolation.

In Eq. (9), $TH^{-1}G$ represents the added fluid mass matrix. For low-frequency vibrations, this matrix can accurately reflect the inertial effect of fluid, but for high-frequency vibrations, $TH^{-1}G$ overestimates the added inertia of fluid. Therefore, it is necessary to modify $TH^{-1}G$ to accurately analyze motion of the coupled system. Here, we only give a modification method for a baffled finite plate, as shown in Fig. 2.

First, compute singular value decomposition of $TH^{-1}G$, i.e.

$$TH^{-1}G = USV^{\mathrm{T}}, \tag{10}$$

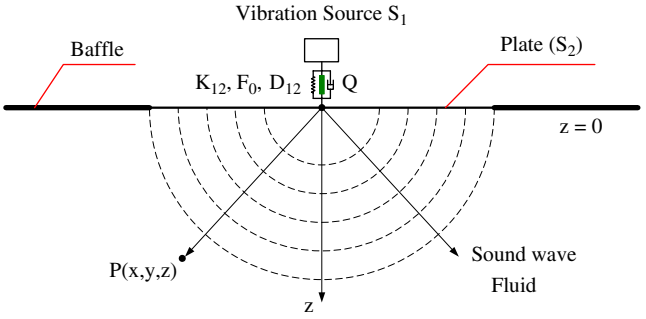

Fig. 2. Rigidly baffled finite plate and active vibration isolation.

where U, V, S are, respectively, the unitary matrices and the singular value matrix. Next, find one accurate wet natural frequency of the plate by solving the coupled finite element model and the boundary element model that is constructed in the frequency domain from the Helmholtz integral equation with $g(Q, P) = \exp(-j\omega r/c)/4\pi r$. Accuracy of the wet frequency can be guaranteed because the sound speed has been taken into account. Then, multiply S with a weighting matrix W whose elements are$\{\varepsilon(k)^{\alpha} | \varepsilon(k) = 0.1 + k\delta,\ 0 \leqslant k \leqslant N_s,\ N_s\delta = 0.9.\}$, N_s is the number of singular values, α is a constant determined from the wet natural frequency. Finally, give the modified added fluid mass matrix $\tilde{M} = USWV^{\mathrm{T}}$ with $W = \mathrm{diag}([1, \ldots, 0.1^{\alpha}])$. Therefore, motion equations of the fluid–plate coupled system with modified mass matrix can be given as follows:

$$\begin{bmatrix} M_{1i} & M_{1c} & O \\ M_{1c}^{\mathrm{T}} & M_{1f} & O \\ O & O & M_z + \Phi^{\mathrm{T}}\tilde{M}\Phi \end{bmatrix} \begin{Bmatrix} \ddot{x}_{1i} \\ \ddot{x}_{1f} \\ \ddot{Z} \end{Bmatrix} + \begin{bmatrix} D_{1i} & D_{1c} & O \\ D_{1c}^{\mathrm{T}} & D_{1f} + D_{12} & -D_{12}\Phi_f \\ O & -\Phi_f^{\mathrm{T}} D_{12} & D_z \end{bmatrix} \begin{Bmatrix} \dot{x}_{1i} \\ \dot{x}_{1f} \\ \dot{Z} \end{Bmatrix}$$
$$+ \begin{bmatrix} K_{1i} & K_{1c} & O \\ K_{1c}^{\mathrm{T}} & K_{1f} + K_{12} & -K_{12}\Phi_f \\ O & -\Phi_f^{\mathrm{T}} K_{12} & K_z \end{bmatrix} \begin{Bmatrix} x_{1i} \\ x_{1f} \\ Z \end{Bmatrix} = \begin{Bmatrix} F_{1i} \\ -F_c \\ \Phi_f^{\mathrm{T}} F_c \end{Bmatrix}. \tag{11}$$

To compute the induced sound pressure in the far field, the sound speed c should be a finite value. For the baffled plate in Fig. 2, the instantaneous pressure at a far-field point $p(x, y, z)$ can be given by the Rayleigh integration:

$$p(x, y, z, t) = \frac{\rho}{2\pi} \int_{\Gamma} \frac{a(x_0, y_0, t - r/c)}{r} \mathrm{d}\Gamma, \quad r = \sqrt{(x - x_0)^2 + (y - y_0)^2 + z^2}, \tag{12}$$

where $(x_0, y_0, 0)$ is an arbitrary point located on the plate (x, y, z) is a point located in the semi-infinite space, as shown in Fig. 2, $a(x_0, y_0, t)$ is the acceleration of $(x_0, y_0, 0)$ at the time t, Γ stands for the surface of the plate.

3. Active vibration isolation

3.1. Velocity feedback

In Fig. 2, vibration of the coupled system is induced by the vibration source. Hence, the natural vibration of the coupled system will be excited when the excitation force is nonstationary. To suppress the natural vibration of the coupled system, vibration velocity of the plate can be measured and used as a feedback signal to generate counter forces acting on the plate. Suppose the feedback velocity is $\dot{x}_{2f}$, the control forces can be given as

$$F_c = -L\dot{x}_{2f} = -L\Phi_f\dot{Z}, \tag{13}$$

where L is the gain matrix. Substituting Eq. (13) into Eq. (11), one can have

$$\begin{bmatrix} M_{1i} & M_{1c} & O \\ M_{1c}^{\mathrm{T}} & M_{1f} & O \\ O & O & M_z + \Phi^{\mathrm{T}}\tilde{M}\Phi \end{bmatrix} \begin{Bmatrix} \ddot{x}_{1i} \\ \ddot{x}_{1f} \\ \ddot{Z} \end{Bmatrix} + \begin{bmatrix} D_{1i} & D_{1c} & O \\ D_{1c}^{\mathrm{T}} & D_{1f} + D_{12} & (L - D_{12})\Phi_f \\ O & -\Phi_f^{\mathrm{T}} D_{12} & D_z + \Phi_f^{\mathrm{T}} L \Phi_f \end{bmatrix} \begin{Bmatrix} \dot{x}_{1i} \\ \dot{x}_{1f} \\ \dot{Z} \end{Bmatrix} + \begin{bmatrix} K_{1i} & K_{1c} & O \\ K_{1c}^{\mathrm{T}} & K_{1f} + K_{12} & -K_{12}\Phi_f \\ O & -\Phi_f^{\mathrm{T}} K_{12} & K_z \end{bmatrix} \begin{Bmatrix} x_{1i} \\ x_{1f} \\ Z \end{Bmatrix} = \begin{Bmatrix} F_{1i} \\ O \\ O \end{Bmatrix}. \tag{14}$$

According to the damping matrix in Eq. (14), velocity feedback can increase the damping ratio of S_2 [16,17]. As a result, vibration of the plate and its sound radiation can be suppressed.

3.2. Adaptive control

When structures are excited by harmonic excitations, there will be harmonic components in the radiated sound. In active vibration/sound control, adaptive algorithms are frequently used to cancel these harmonic components although there are many other control methods. In this section, adaptive vibration cancellation and its role in sound suppression are discussed. Since the behavior of the coupled fluid–plate system under adaptive control is the focus of this section, only the adaptive control algorithm—LMS is adopted here.

According to Eqs. (13) and (14), vibration of S_2 is controlled by feedback of the measured velocity $\dot{x}_{2f}$. Similarly, the adaptive control of vibration of S_2 can also be realized by the measured velocity $\dot{x}_{2f}$. However, for the simplicity of discussion, the measured acceleration instead of velocity will be used in the adaptive suppression of sound radiation of S_2. Suppose the discrete form of Eq. (11) and the observed acceleration $\ddot{x}_{2f}$ are expressed by

$$\begin{aligned} \varphi(x_1(t_k), \dot{x}_1(t_k), x_1(t_{k+1}), \dot{x}_1(t_{k+1}), Z(t_k), \dot{Z}(t_k), Z(t_{k+1}), \dot{Z}(t_{k+1})) &= B_1 F_{1i}(t_k) + B_2 F_c(t_k) \\ \ddot{x}_{2f}(t_k) &= \vartheta(Z(t_k), \dot{Z}(t_k), F_{1i}(t_k), F_c(t_k)), \end{aligned} \tag{15}$$

where t_k is the discrete time, B_1, B_2 are the load matrices. The adaptive control algorithm can be given as follows:

(1) Weight updating:

$$\begin{aligned} w_1(t_{k+1}) &= w_1(t_k) - \mu \sin(2\pi f t_k)\ddot{x}_{2f}(t_k), \\ w_2(t_{k+1}) &= w_2(t_k) - \mu \cos(2\pi f t_k)\ddot{x}_{2f}(t_k), \end{aligned} \tag{16}$$

where $w_1(t_k)$, $w_2(t_k)$ are weights, μ is a constant, f is the frequency of the disturbance force.

(2) Control forces:

$$F_c(t_k) = w_1(t_k)\sin(2\pi f t_k) + w_2(t_k)\cos(2\pi f t_k). \tag{17}$$

The control forces are so constructed to reduce the acceleration $\ddot{x}_{2f}$.

3.3. Sound radiation control

Eqs. (13) and (17) imply that sound radiation of the plate is not controlled directly because the control forces are constructed to minimize the measured vibration of the plate, but not the radiated sound in the far field. The drawback of this indirect control is that sound pressure in the far field may not be suppressed as much as the vibration of the plate. Hence, in order to suppress sound pressure sufficiently, $p(x, y, z)$ should be minimized directly. However, sound pressure in the far field cannot be measured for a practical control system.

From Eq. (12), sound pressure in the near field can be given approximately by

$$p(x,y,z,t) \approx \frac{\rho}{2\pi}\int_{\Gamma}\frac{a(x_0,y_0,t)}{r}\,\mathrm{d}\Gamma. \tag{18}$$

Therefore, the near field sound pressure is approximately equal to the weighted integration of acceleration of the plate, which implies that distributed acceleration summation is suitable for the measurement of the near field sound pressure, and minimizing the integration of acceleration may have the same effect as minimizing the near field sound pressure. Hence, the updating of weights in Eq. (16) can be rewritten as

$$\begin{aligned} w_1(t_{k+1}) &= w_1(t_k) - \mu\,\sin(2\pi f t_k)\sum_{i,j}\ddot{x}_2(i,j,t_k),\\ w_2(t_{k+1}) &= w_2(t_k) - \mu\,\cos(2\pi f t_k)\sum_{i,j}\ddot{x}_2(i,j,t_k), \end{aligned} \tag{19}$$

where $\ddot{x}_2(i,j,t_k)$ is the acceleration of the node (i,j) of the plate. It should be noted that the distance r in Eq. (18) has been treated as a constant in forming Eq. (19).

4. An example on FE/BE modeling

Consider a plate with cross-stiffeners on one side and a vibration model of two DOFs, as shown in Fig. 3. The 2-DOF model and the plate are connected at one cross-point (there are totally nine possible cross-points). The plate is simply supported and rigidly baffled. The flat side of the plate is coupled with the fluid. Dimensions and physical properties of the stiffened plate and the fluid are given in Table 1. Moreover, parameters of the 2-DOF vibration model are given as follows: $m_1 = m_2 = 1\,\mathrm{kg}$, $k_1 = 24{,}674\,\mathrm{N/m}$, $k_2 = 3948\,\mathrm{N/m}$, $d1 = 15.71\,\mathrm{N\,s/m}$, and $d2 = 31.4\,\mathrm{N\,s/m}$.

The plate is modeled with 256 shell elements and the stiffeners are modeled with beam elements. The 2-DOF model is connected at the cross-point 9 to the finite element model of the stiffened plate (Fig. 3). For the stiffened plate, the first 30 dry modes (without fluid) are derived and used to form a coupled model according to Eq. (5) or Eq. (11). The first six mode shapes of the stiffened plate are shown in Fig. 4 and the first 14 natural frequencies are listed in Table 2.

The fluid at the fluid–plate interface is modeled with boundary elements (BEs), which are in coincidence with the finite elements (FEs) of the plate. Having obtained the FE and BE models, the motion equations of

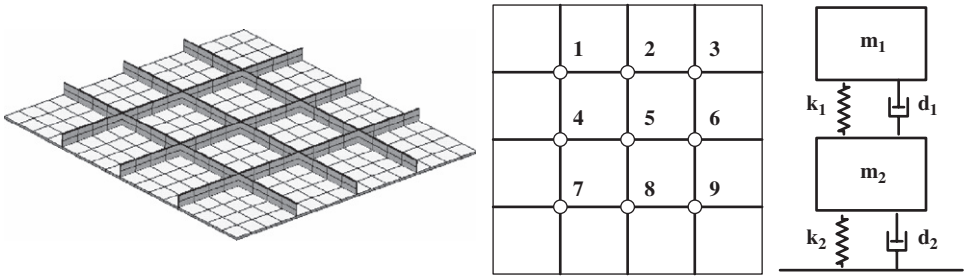

Fig. 3. Finite element model of the plate with cross-stiffeners (left) and the 2-dof vibration model (right).

Table 1
Dimensions and physical properties

	Dimension (m)	Density (kg/m^3)	Young's modulus (N/m^2)	Poisson's ratio	Sound velocity (m/s)
Plate	$0.8\times0.8\times0.003$	7850	2.1×10^{11}	0.3	–
Stiffener	$0.8\times0.018\times0.003$	7850	2.1×10^{11}	0.3	–
Fluid	–	1000	–	–	1500

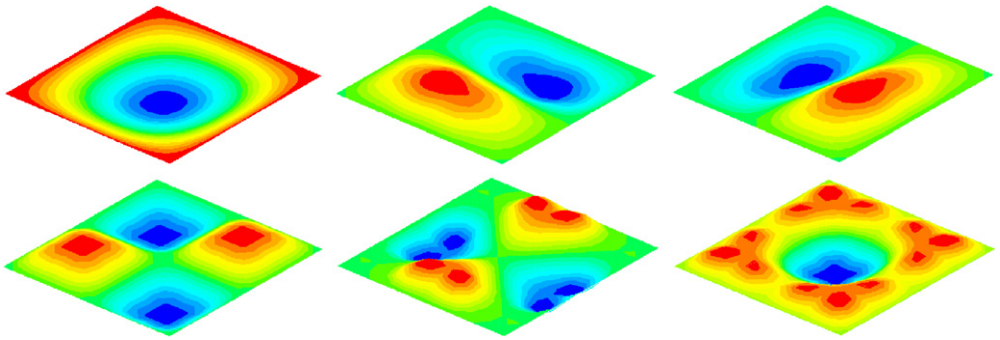

Fig. 4. The first six mode shapes of the stiffened plate.

Table 2
Undamped natural frequencies and eigenvalues of the coupled system

No.	Frequencies of dry modes (Hz)	Frequencies of wet modes (Hz)		Eigenvalues (damping ratio = 10%)
–	Stiffened plate	Based on the Laplace equation and modified	Based on the Helmholtz equation	$-1.2\pm6.8i$ $-3.8\pm35.8i$
1	61.2	17.3	17.3	$-0.7\pm17.3i$
2	167.4	67.9	67.6	$-4.2\pm67.9i$
3	167.4	67.9	67.6	$-4.2\pm67.9i$
4	232.5	107.8	107.4	$-7.6\pm107.6i$
5	329.3	151.5	151.4	$-10.5\pm151.4i$
6	329.3	160.0	159.5	$-11.7\pm160.0i$
7	353.1	182.2	181.8	$-14.1\pm181.6i$
8	353.1	182.2	181.8	$-14.1\pm181.6i$
9	378.5	215.4	216.6	$-18.3\pm214.6i$
10	380.3	227.2	228.6	$-19.9\pm226.4i$
11	385.6	230.2	231.6	$-20.2\pm229.4i$
12	385.6	230.2	231.6	$-20.2\pm229.4i$
13	409.8	238.6	239.8	$-20.8\pm237.7i$
14	411.6	240.5	241.5	$-20.5\pm239.6i$

the coupled system can be obtained according to Eq. (9). To modify the added mass matrix and guarantee to some extent the accuracy of frequencies of the coupled system, singular values are weighted by $\mathrm{diag}([1,\ldots,0.1^{\alpha}])$ with $\alpha = 1.3$, which is determined from the 14th wet frequency of the stiffened plate. The wet frequencies are accurately computed from the Helmholtz equation, which are also listed in Table 2 for the purpose of comparison. Eigenvalues of the coupled system are given as well in Table 2, in which damping ratios of all modes of the plate are assumed to be 10%. In terms of the computed results, the modified wet frequencies are in good consistency with the exact ones.

As can be seen from the table, the inertial effect of the fluid has substantially reduced high-order frequencies of the stiffened plate. Hence, active isolation should be based on the coupled fluid–structure system.

5. Simulation on active isolation

5.1. Random disturbance

Suppose m_1 is excited by a random force, in this circumstance, responses of the stiffened plate are also random. To reduce vibration of the plate and its sound radiation, active isolation is expected to suppress natural modes of the plate. Therefore, velocity feedback is used and the control force is exerted on m_2 and the

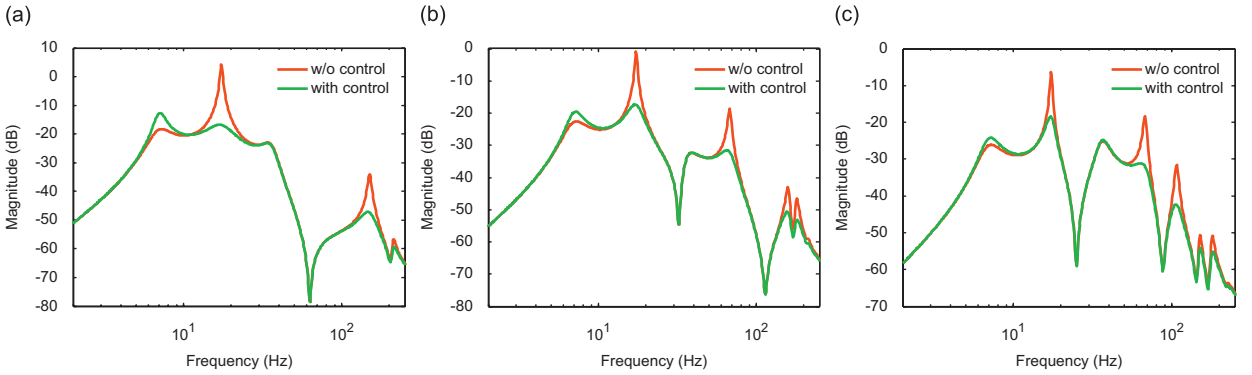

Fig. 5. Frequency responses at three cross-points: (a) At the cross-point 5. (b) At the cross-point 8 (c). At the cross-point 9.

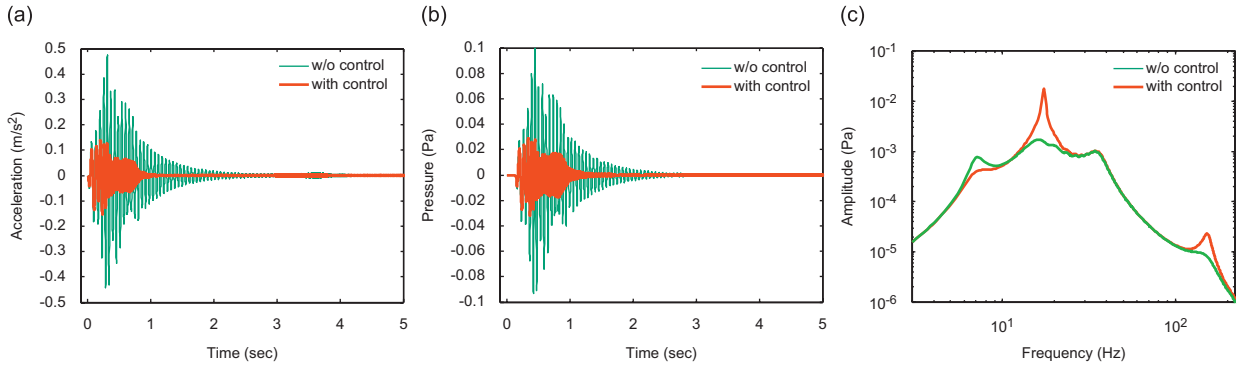

Fig. 6. Acceleration responses at the cross-point 5 and sound pressure at (0, 0, 200 m): (a) Acceleration. (b) Sound pressure. (c) Spectra of sound pressure.

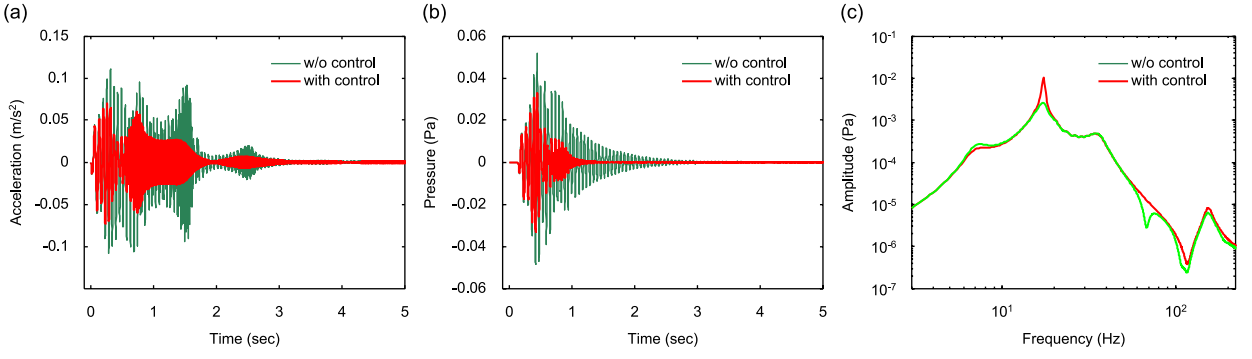

Fig. 7. Acceleration responses at the cross-point 9 and sound pressure at (0, 0, 200 m): (a) Acceleration. (b) Sound pressure. (c) Spectra of sound pressure.

plate simultaneously. Frequency response function between the excitation force and acceleration of the mount position of m_2 can be computed according to Eq. (14). Fig. 5 depicts frequency responses between the excitation force and accelerations of three cross-points. As can be seen, different modes are observed at different cross-points. Only symmetric modes can be observed at the cross-point 5. More modes are excited and observed at the cross-point 9, which can also be verified by simply examining mode shapes in Fig. 4. With active isolation, observed natural modes are suppressed and peaks of the frequency responses are correspondingly reduced substantially, as shown in the figure.

Sound pressure in the far field is related to the surface vibration of the plate, but the attenuation of sound pressure is not the same as that of vibration [18]. Figs. 6 and 7 have shown the time histories of acceleration and sound pressure. The responses are induced by a chirp force acting on m_1, frequency of which varies from 10 to 250 Hz within 5 s. According to the transient responses, it is demonstrated that active isolation can reduce acceleration responses as well as the far-field sound pressure, but there may be little similarity in envelops of acceleration and sound pressure. Moreover, spectra in Figs. 6 and 7 indicate that the far-field sound pressure is irrelative to unsymmetric modes. Especially, the 2–5th plate modes have no contribution to the far-field sound pressure. For weakly controllable modes, peak suppression is correspondingly small under the same feedback gain. This implies that sound pressure control is related to locations where the control force acts. Therefore, suppressing acceleration is not the same as sound pressure control.

5.2. Harmonic disturbance

When m_1 is excited by a harmonic force, forced vibrations will occur in the stiffened plate and it will radiate sound to the far field. As a result, sound pressure in the far field will oscillate at a single frequency. In this section, adaptive vibration isolation based on Eqs. (16) and (19), is simulated to reveal the relation between vibration control and the sound suppression. In the simulation, the 2-DOF model is mounted, respectively, at the cross-points 5 and 9. Active isolation is then adjusted according to the principle that the local acceleration response or the summed acceleration response is minimized. Let m_1 be excited by a force of 150 Hz, the acceleration responses and sound pressure with/without adaptive control are then simulated and given, respectively, in Fig. 8. In Fig. 8(a), the forced acceleration responses are in fact composed of the transient and the steady-state responses, from which we can see that the acceleration at the cross-point 5 is well suppressed after the adaptive isolation while sound pressure in the far field is not reduced as much as the acceleration response, as shown in Fig. 8(b). This indicates the minimization of local accelerations may not result in sufficient attenuation of the far-field sound pressure. In Fig. 8(c), the summed acceleration is substantially reduced after the adaptive isolation and the far-field sound pressure shown in Fig. 8(d) is also sufficiently attenuated, which implies the isolation based on summed acceleration minimization has almost the same result as the direct sound pressure control.

The distribution of sound pressure in the near field is of much interest. Let the 2-DOF model be mounted at the cross-point 9 and excited by a force of 40 Hz. Active isolation is then started to minimize the summed acceleration according to Eq. (19). The controlled sound pressure measured at $(0, 0, 1)$, $(0, 1, 1)$, $(1, 0, 1)$, $(0, -1, 1)$, $(-1, 0, 1)$, $(1, 1, 1)$, $(1, -1, 1)$, $(-1, -1, 1)$, $(-1, 1, 1)$, and $(-0.5, -0.5, 1)$ is shown in Fig. 9(a), from which we can see that the sound pressure enters a stable stage after almost 0.8 s adaptation. Fig. 9(b) gives the distribution of sound pressure without active vibration isolation (AVI off), and the distribution of sound pressure under active vibration isolation (AVI on) is given in Fig. 9(c). The sound pressure surfaces are generated, respectively, by interpolation of the ten measured pressure values. The contours of sound pressure on the $1\,\mathrm{m} \times 1\,\mathrm{m}$ area are also shown in Figs. 9(b) and (c), from which we can see that the center of the pressure contour under AVI deviates apparently from the geometric center $(0, 0, 1)$ and the sound pressure becomes lower around $(0.2, 0.2, 1)$ where the 2-DOF model is mounted. Therefore, the effect of active isolation on the distribution of pressure is evident.

6. Conclusions

Active vibration isolation and the relevant underwater sound radiation of structures have been discussed. In this paper, FEM/BEM is adopted to deal with the interaction between fluid and structures and to establish motion equations of the coupled system. During the modeling, modal truncation and the inertia coupling of structures and the fluid are considered to derive a model of sufficiently small number of DOFs. A procedure has been presented to modify the added mass matrix of the fluid to guarantee accuracy of the dynamic characteristics of the model at low frequencies. This model is constructed particularly for investigating problems of vibration and sound control in the time domain because of its flexibility in dealing with nonlinear control.

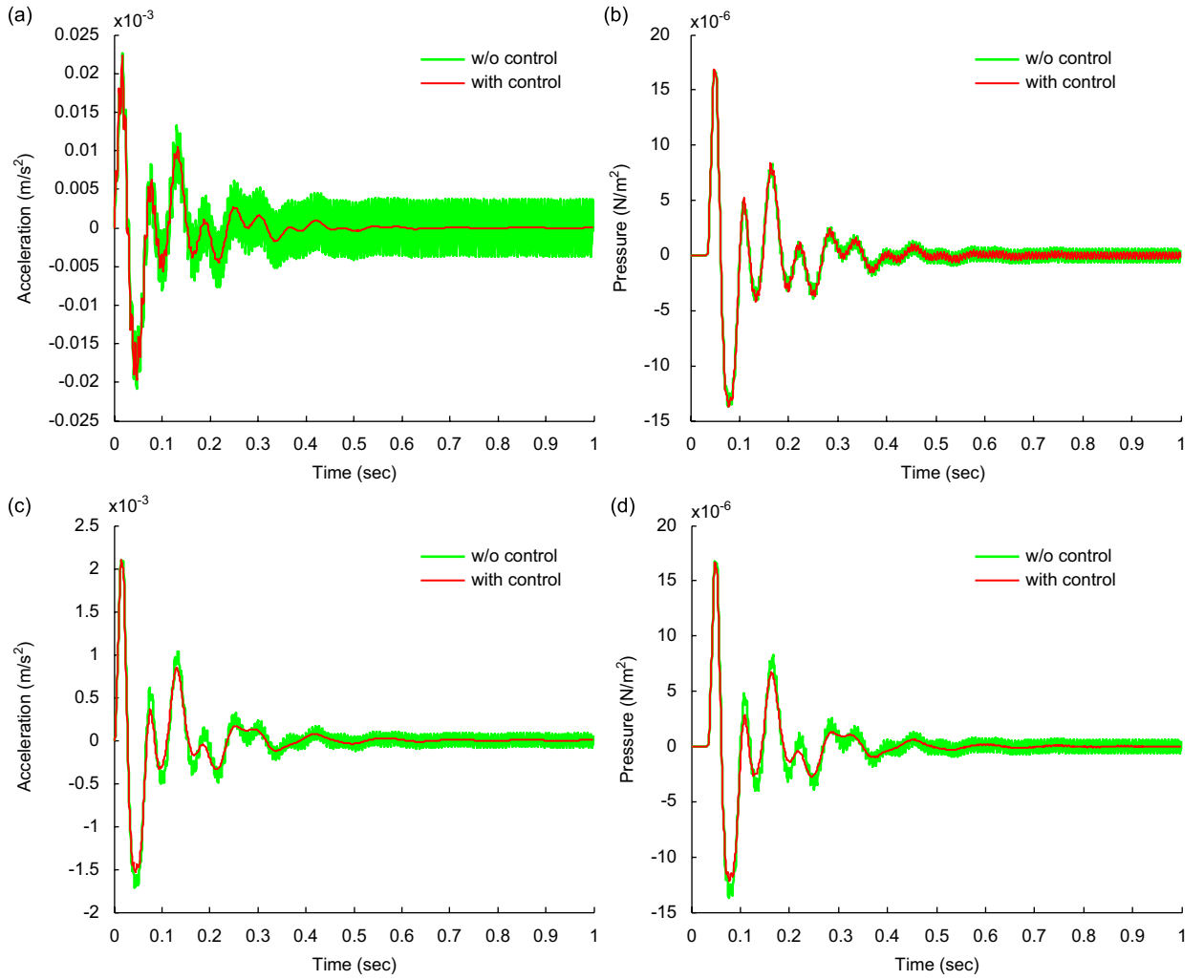

Fig. 8. Acceleration responses and the sound pressure at (0, 0, 50 m): (a) Acceleration at the cross-point 5. (b) Sound pressure. (c) Summed acceleration. (d) Sound pressure.

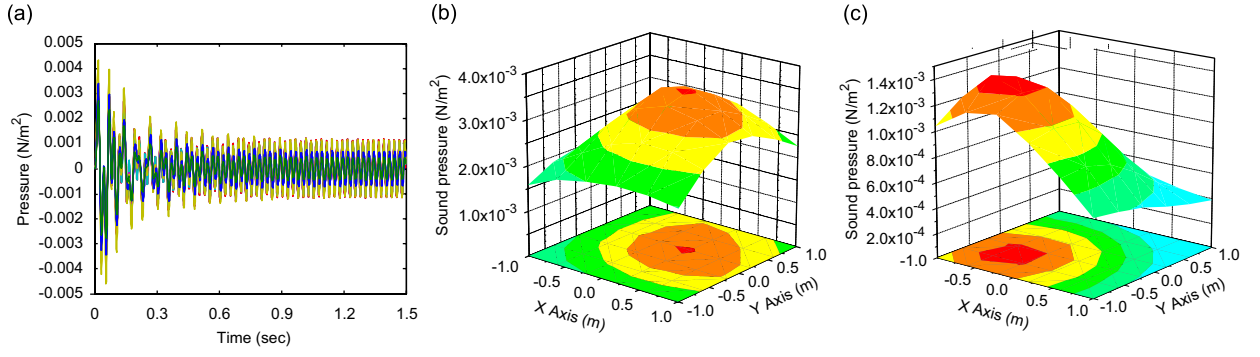

Fig. 9. Sound pressure at selected points on the plane $z = 1$ (active isolation at the cross-point 9): (a) Pressure history (40 Hz). (b) Pressure distribution (AVI off). (c) Pressure distribution (AVI on).

The interaction between fluid and structures has changed the natural frequencies and active control should be based on the coupled system. Vibration control and sound radiation of a stiffened plate, to which a 2-DOF vibration model is connected, has been simulated. The results have demonstrated that suppression of summed vibration can result in smaller sound radiation than the suppression of local vibration only. Suppression of summed vibration has almost the same role as the direct control of sound pressure. However, distributed measurement of vibration is needed in this circumstance. Vibration reduction does not definitely lead to attenuation of sound radiation, which is attributed to the fact that sound pressure in the far field is affected only by certain vibration modes. Therefore, active vibration isolation is not the same as sound radiation control unless special control methods are considered.

Acknowledgment

This work was supported by the NSF of China (Grant no. 10672099).

References

[1] B. Nolte, L. Gaul, Sound energy flow in the acoustic near field of a vibrating plate, *Mechanical Systems and Signal Processing* 10 (3) (1996) 351–364.
[2] H. Nelisse, O. Beslin, J. Nicolas, A generalized approach for the acoustic radiation from a baffled or unbaffled plate with arbitrary boundary conditions, immersed in a light or heavy fluid, *Journal of Sound and Vibration* 211 (2) (1998) 207–225.
[3] H.H. Bleich, M.L. Baron, Free and forced vibration of an infinitely long cylindrical shell in a infinite acoustic medium, *Journal of Applied Mechanics* (2) (1954) 167–177.
[4] R.H. Lyon, Sound radiation from a beam attached to plate, *Journal of the Acoustical Society of America* (34) (1962) 1265–1268.
[5] H.K. Lee, Y.S. Park, A near-field approach to active control of sound radiation from a fluid-loaded rectangular plate, *Journal of Sound and Vibration* 196 (5) (1996) 579–593.
[6] C.C. Cheng, J.K. Wang, Structural acoustic response reduction of a fluid-loaded beam using unequally spaced concentrated masses, *Applied Acoustics* 54 (4) (1998) 291–303.
[7] V.V. Varadan, Z. Wu, S.Y. Hong, V.K. Varadan, Active control of sound radiation from a vibrating structure, *Ultrasonics Symposium*, 1991, pp. 991–994.
[8] C.R. Fuller, Active control of sound transmission/radiation from elastic plates by vibration inputs: I. analysis, *Journal of Sound and Vibration* 136 (1990) 1–15.
[9] Sheng Li, Deyou Zhao, Numerical simulation of active control of structural vibration and acoustic radiation of a fluid-loaded laminated plate, *Journal of Sound and Vibration* 272 (2004) 109–124.
[10] P.T. Chen, Vibrations of submerged structures in a heavy acoustic medium using radiation modes, *Journal of Sound and Vibration* 208 (1) (1997) 55–71.
[11] C.G. Everstine, F.M. Henderson, Coupled finite element/boundary element approach for fluid–structure interaction, *Journal of the Acoustical Society of America* 87 (5) (1990) 1938–1946.
[12] G.Y. Yu, Symmetric collocation BEM/FEM coupling procedure for 2-D dynamic structural–acoustic interaction problems, *Computational Mechanics* (29) (2002) 191–198.
[13] Z. Tong, Y. Zhang, Z. Zhang, H. Hua, Dynamic behavior and sound transmission analysis of a fluid–structure coupled system using the direct-BEM/FEM, *Journal of Sound and Vibration* 299 (2007) 645–655.
[14] A. Ergin, The response behaviour of a submerged cylindrical shell using the doubly asymptotic approximation method (DAA), *Computers and Structures* 62 (6) (1997) 1025–1034.
[15] T.L. Geers, A.A. Fellipa, Doubly asymptotic approximation for vibration analysis of submerged structures, *Journal of the Acoustical Society of America* 73 (4) (1983) 1152–1159.
[16] M.E. Johnson, S.J. Elliott, Active control of sound radiation using volume velocity cancellation, *Journal of the Acoustical Society of America* 98 (4) (1995) 2174–2186.
[17] J. Holterman, T.J.A. de Vries, Active damping based on decoupled collocated control, *IEEE/ASME Transactions on Mechatronics* 10 (2) (2005) 135–145.
[18] F. Fahy, *Sound and Structural Vibration*, Academic Press Inc., London, 1985.